---- Supporting Information ----

Exploring Multi-Transition-Metal NASICON Frameworks as High-Performance Cathodes for Sodium-Ion Batteries

Santosh Behara[a,b], Achinthya Krishna Bheemaguli[b], Gopalakrishnan Sai Gautam*[b]

[a]Department of Metallurgical and Materials Engineering, National Institute of Technology Andhra Pradesh, Tadepalligudem 534101, India

[b]Department of Materials Engineering, Indian Institute of Science, Bengaluru 560012, India

E-mail: saigautamg@iisc.ac.in

Methods

We performed all spin-polarized density functional theory (DFT) calculations using the Vienna ab initio simulation package.[1,2] We used the projector augmented-wave method[3,4] to describe the core electrons and compiled the potentials used in **Table S1**. To account for the strong electronic correlations of the transition metal (TM) *d* electrons, we employed the Hubbard *U* corrected strongly constrained and appropriately normed (i.e., SCAN+*U*) functional.[5,6] We set the effective *U* values as follows: 3.1 eV for Fe, 2.7 eV for Mn, and 0 eV for Cr, based on prior benchmarks (**Table S2**).[7–9] We used rhombohedral $Na_3V_2(PO_4)_3$ as the starting structure for our calculations, as obtained from the inorganic crystal structure database (ICSD).[10] We truncated the plane-wave basis set at a kinetic energy cutoff of 520 eV, sampled the irreducible Brillouin zone using Γ-centered Monkhorst-Pack[11] *k*-point meshes with a minimum density of 48 *k*-points per Å, and integrated the Fermi surface with Gaussian smearing of width 0.05 eV. We fully relaxed the cell volumes, cell shapes, and ionic positions of all structures considered, without preserving any underlying symmetry, until the residual forces fell below |0.03| eV/Å and the total energies converged within 0.01 meV. We initialized all TMs in high-spin ferromagnetic configurations to approximate their ground-state magnetic ordering. We

Downloaded from http://pubs.acs.org/aamick/article-supplement/5249728/pdf/am-2026-11510n_si_001/ by INDIAN INST OF SCIENCE user on 07 August 2026

evaluated the electronic structures by calculating the total and projected densities of states (DOS) with denser 96 *k*-point per Å meshes using the tetrahedron method with Blöchl corrections.[12]

For calculating the average (de)intercalation voltages of Na in the sodium superionic conductor (NASICON) frameworks considered, we modeled the electrochemical intercalation process as a reversible reaction,

$$Na_yTM_2(PO_4)_3 + (x-y)Na^+ + (x-y)e^- \overset{-\Delta G^0}{\longleftrightarrow} Na_xTM_2(PO_4)_3 \quad (1)$$

Here, y and x are the charged and discharged Na compositions in the NASICON framework, respectively. We approximated the Gibbs free energy change ΔG^0 using DFT total energies and neglected pV and entropic terms. Subsequently, we calculated the average intercalation voltage as,[13]

$$V = -\frac{\Delta G^0}{(x-y)F} \approx -\frac{E(Na_xTM_2(PO_4)_3) - [E(Na_yTM_2(PO_4)_3) + (x-y)\mu_{Na}]}{(x-y)F} \quad (2)$$

where μ_{Na} represents the chemical potential of bulk sodium metal in its ground state body centered cubic structure, and F is the Faraday's constant.

We evaluated the phase behavior at 0 K for all intermediate Na-compositions within each NASICON framework considered via DFT-calculated formation energies, $E_f(x)$, with $1 \leq x \leq 4$. For calculating $E_f(x)$, we used the fully charged ($E(Na_1TM_2(PO_4)_3)$) and fully discharged ($E(Na_4TM_2(PO_4)_3)$) compositions as references.

$$E_f(x) = E(Na_xTM_2(PO_4)_3) - \left(\frac{4-x}{3}\right)E(Na_1TM_2(PO_4)_3) - \left(\frac{x-1}{3}\right)E(Na_4TM_2(PO_4)_3) \quad (3)$$

At each intermediate Na composition, we systematically generated symmetrically distinct Na/vacancy orderings using the pymatgen library,[14] in Na compositional steps (Δx) of 1 across the compositional range $1 \leq x \leq 4$. We used the primitive cell of the NASICON structure, containing 2 f.u., for performing our enumerations. Upon enumeration, we used the Ewald

Downloaded from http://pubs.acs.org/aamick/article-supplement/5249728/pdf/am-2026-11510n_si_001/ by INDIAN INST OF SCIENCE user on 07 August 2026

summation technique[15] to rank structures based on electrostatic energies, calculated by assigning point charges of +1, +5, and -2 for the Na, P, and O, respectively, while the TM was assigned an oxidation state that would render the overall structure charge-neutral. Upon electrostatic ranking, we chose the 10 lowest energy structures for further DFT calculations at each Na composition.

For assessing the overall thermodynamic stability of all NASICON compositions considered, we constructed the 0 K convex hull of the Na–Mn–Cr–Fe–P–O six component chemical space using DFT-calculated energies and computed the associated energy above the convex hull (E_{hull}) for NASICON compositions considered. For constructing the 6D convex hull, we incorporated all relevant elemental, binary, ternary, quaternary, and quinary ordered structures, as available in the ICSD to ensure a comprehensive stability evaluation.[10] Since only DFT-calculated total energies at 0 K were used to construct the convex hull, the resulting phase diagrams do not explicitly account for entropic or pV contributions.

To estimate the Na^+ migration barriers (E_m), we adopted a two-step procedure using the fully sodiated $Na_4TM_2(PO_4)_3$ compositions as the starting point for all nine NASICON systems. First, we used the multi atomic cluster expansion (MACE) universal machine learned interatomic potential, namely the MACE-MP-0 potential[16] as integrated within the atomic simulation environment[17] to perform nudged elastic band (NEB) calculations.[18] We relaxed initial and final endpoints with a quasi-Newton optimizer until forces dropped below |0.05| eV/Å over a maximum of 1000 steps. We generated seven intermediate images using the image dependent pair potential interpolation method[19] with a spring constant of 5 eV/Å^2, similar to our previous work.[20] We optimized the minimum energy path with the NEB method[21] until band forces converged below |0.05| eV/Å, using the Broyden–Fletcher–Goldfarb–Shanno optimizer.[22] All MACE-based NEB calculations employed the "large" MACE-MP-0 model with maximal message equivariance (i.e., L_max = 2). Second, we re-optimized the MACE-

Downloaded from http://pubs.acs.org/aamick/article-supplement/5249728/pdf/am-2026-11510n_si_001/ by INDIAN INST OF SCIENCE user on 07 August 2026

relaxed endpoints using DFT with fixed lattice parameters and relaxing ionic positions. We applied convergence thresholds of 0.01 meV for energy and |0.03| eV/Å for forces. Subsequently, we refined the migration path by combining MACE-relaxed intermediate image coordinates with DFT-optimized endpoints as inputs for full DFT-NEB calculations. We carried out the DFT-NEB simulations using the Perdew-Burke-Ernzerhof version of the generalized gradient approximation functional,[23] to reduce computational costs while retaining robust qualitative trends.[24]

Table S1: Projector augmented-wave potentials used to describe the core electrons for each atomic species in DFT calculations.

Element	Potential
Na	Na_pv 19Sep2006
Mn	Mn_pv 02Aug2007
Cr	Cr_pv 02Aug2007
Fe	Fe_pv 02Aug2007
P	P 06Sep2000
O	O 08Apr2002

Table S2: Hubbard *U* values used in this study along with the SCAN functional. The *U* Values are taken from literature.

Element	***U*** **(eV)**
Mn	2.7
Cr	0
Fe	3.1

Downloaded from http://pubs.acs.org/aamick/article-supplement/5249728/pdf/am-2026-11510n_si_001/ by INDIAN INST OF SCIENCE user on 07 August 2026

Table S3: DFT-computed lattice parameters of all Na ground-state configurations of binary and ternary sodium superionic conductor (NASICON) cathodes investigated in this work. Here, NMP, NCP, NFP, NMCP, NCFP, NFMP, NMCFP, NCFMP, and NFMCP denote $Na_xMn_2(PO_4)_3$, $Na_xCr_2(PO_4)_3$, $Na_xFe_2(PO_4)_3$, $Na_xMnCr(PO_4)_3$, $Na_xCrFe(PO_4)_3$, $Na_xFeMn(PO_4)_3$, $Na_xMnCr_{0.5}Fe_{0.5}(PO_4)_3$, $Na_xCrFe_{0.5}Mn_{0.5}(PO_4)_3$, and $Na_xFeMn_{0.5}Cr_{0.5}(PO_4)_3$, respectively, for x = 1-4.

System	x	Lattice parameters						Volume (Å^3)
		a **(Å)**	***b*** **(Å)**	***c*** **(Å)**	***α*** **(º)**	***β*** **(º)**	***γ*** **(º)**	
NMP	1	8.29	8.29	8.58	61.10	61.10	60.00	423.64
	2	8.44	8.51	8.53	62.34	62.27	59.77	447.08
	3	8.64	8.64	8.72	60.52	60.52	62.38	471.54
	4	8.93	8.92	8.72	60.59	58.44	61.31	491.56
NCP	1	8.39	8.39	8.59	60.79	60.79	60.00	432.51
	2	8.53	8.46	8.65	60.73	60.18	60.30	445.29
	3	8.65	8.65	8.70	59.78	59.78	60.20	459.78
	4	8.93	8.84	8.75	59.85	58.06	60.50	481.89
NFP	1	8.52	8.52	8.76	60.90	60.90	59.99	454.96
	2	8.67	8.64	8.79	60.56	59.97	60.12	467.89
	3	8.74	8.72	8.73	60.02	59.60	60.06	469.50
	4	8.94	8.94	8.68	59.00	58.99	60.00	483.66
NMCP	1	8.16	8.17	8.60	61.51	61.40	60.09	414.77
	2	8.48	8.44	8.65	60.87	60.32	60.24	442.15
	3	8.82	8.66	8.79	60.29	57.96	59.19	464.96
	4	8.94	8.94	8.71	59.13	59.14	60.00	485.72
NCFP	1	8.35	8.35	8.64	61.07	61.09	60.00	432.93
	2	8.54	8.49	8.69	60.39	60.45	60.62	450.50
	3	8.70	8.69	8.71	60.06	59.66	60.08	464.93
	4	8.92	8.91	8.68	59.15	58.76	59.98	479.82
NFMP	1	8.45	8.45	8.67	60.82	60.82	59.99	442.77
	2	8.51	8.48	8.68	60.82	60.29	60.24	447.85
	3	8.71	8.84	8.61	61.54	59.95	59.18	470.77
	4	8.98	8.98	8.74	59.09	59.09	60.00	491.02

Downloaded from http://pubs.acs.org/aamick/article-supplement/5249728/pdf/am-2026-11510n_si_001/ by INDIAN INST OF SCIENCE user on 07 August 2026

NMCFP	1	8.21	8.21	8.60	61.52	61.51	60.00	418.90
	2	8.47	8.52	8.65	60.21	60.71	60.20	444.77
	3	8.81	8.64	8.90	58.92	58.01	60.10	467.77
	4	8.96	8.96	8.73	59.12	59.11	60.00	488.50
NCFMP	1	8.26	8.28	8.59	61.35	61.26	59.89	423.20
	2	8.47	8.53	8.65	60.35	60.75	60.19	446.39
	3	8.68	8.69	8.77	59.85	59.12	60.36	465.04
	4	8.93	8.93	8.68	59.07	59.08	60.00	482.58
NFMCP	1	8.32	8.32	8.63	61.17	61.18	60.02	429.58
	2	8.49	8.54	8.68	60.31	60.54	60.33	448.85
	3	8.71	8.66	8.78	59.17	59.72	60.59	466.96
	4	8.94	8.96	8.67	59.04	59.00	59.97	483.94

Downloaded from http://pubs.acs.org/aamick/article-supplement/5249728/pdf/am-2026-11510n_si_001/ by INDIAN INST OF SCIENCE user on 07 August 2026

Table S4: Comparison of DFT-calculated intercalation voltages with experimentally reported values for representative NASICON cathodes.

Composition	DFT Voltage (V vs. Na/Na^+)	Experimental Voltage (V vs. Na/Na^+)	Remarks
NMP	3.43 (average)	-	Computational prediction. The calculated average voltage agrees well with previous DFT studies of NMP.[25]
NCP	~4.09 (Cr^{4+}/Cr^{3+})	~4.50 (Cr^{4+}/Cr^{3+})	Good agreement with the experimentally observed high-voltage Cr^{4+}/Cr^{3+} redox couple.[26]
NFP	4.07 (average)	~3.30-3.60	Experimental studies confirm reversible Fe-based redox activity.[27]
NMCP	~3.34 (Mn^{3+}/Mn^{2+}), ~3.88 (Mn^{4+}/Mn^{3+}), ~3.88 (Cr^{4+}/Cr^{3+})	~3.40 (Mn^{3+}/Mn^{2+}), ~4.10 (Mn^{4+}/Mn^{3+}), ~4.30 (Cr^{4+}/Cr^{3+})	Good agreement with the experimentally identified Mn- and Cr-redox processes.[28]
NCFP	~2.42 V (Fe^{3+}/Fe^{2+})	~2.6–3.2 V (Fe^{3+}/Fe^{2+})	Experimental Mössbauer spectroscopy confirms Fe^{3+}/Fe^{2+} as the dominant electrochemically active redox couple. No distinct Cr redox activity has been experimentally observed.[29]
NFMP	4.01 (average)	-	Complete absence of redox pairs.[30]
NMCFP	~3.33 (Mn^{3+}/Mn^{2+}), ~3.88 (Mn^{4+}/Mn^{3+})	~3.50 (Mn^{3+}/Mn^{2+}), ~4.20 (Mn^{4+}/Mn^{3+})	The calculated Mn redox voltages agree well with experiment.[31]
NCFMP	~2.88 (Mn/Fe), ~3.95 (Mn^{4+}/Mn^{3+})	~2.70 (Fe^{3+}/Fe^{2+}), ~3.50 (Mn^{3+}/Mn^{2+}), ~4.20 (Mn^{4+}/Mn^{3+})	Experimental studies on related Mn–Fe–Cr NASICONs confirm Fe^{2+}/Fe^{3+} and Mn redox activity.[31]
NFMCP	3.55 (average)	Not yet reported	Computational prediction awaiting experimental validation.

Downloaded from http://pubs.acs.org/aamick/article-supplement/5249728/pdf/am-2026-11510n_si_001/ by INDIAN INST OF SCIENCE user on 07 August 2026

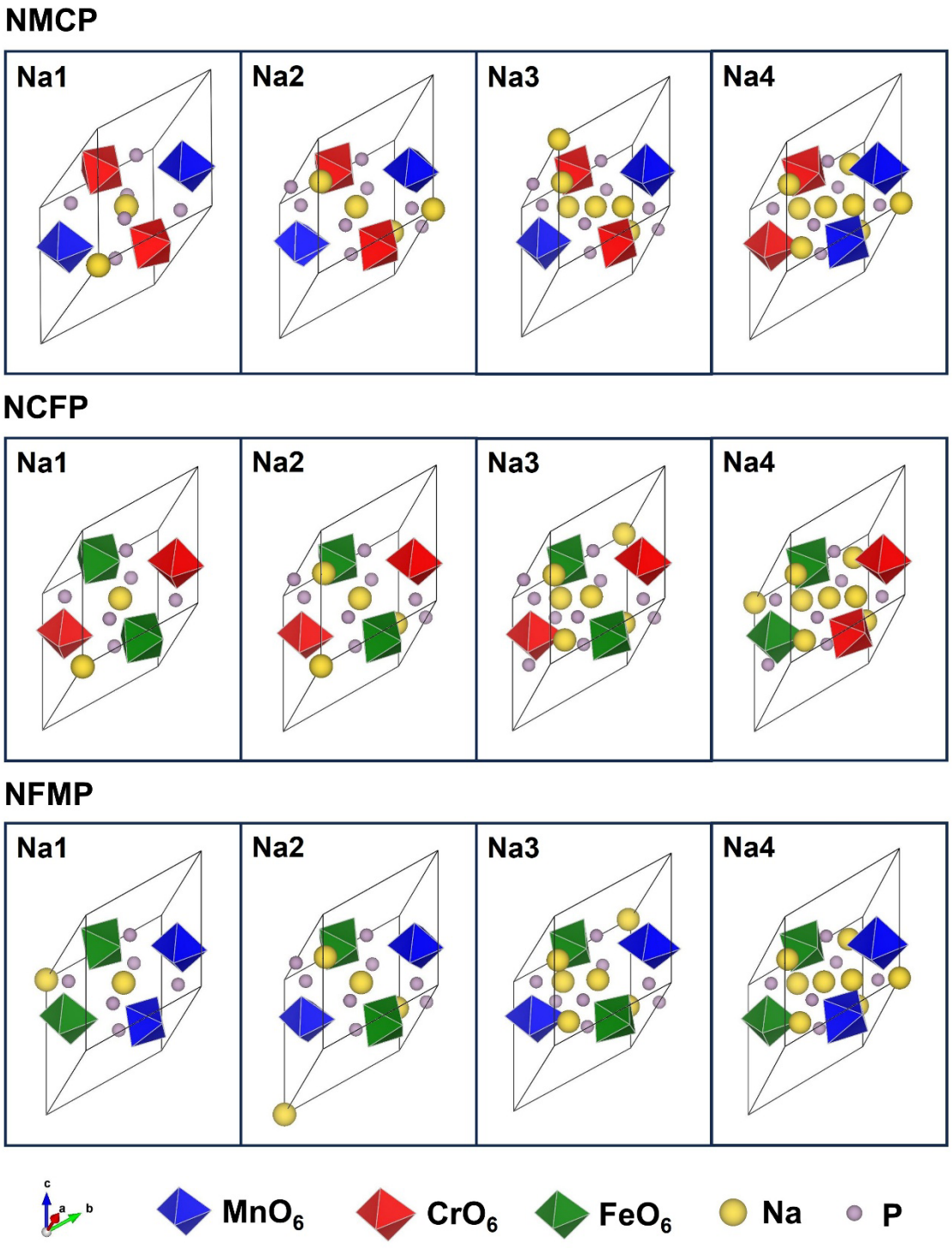

Figure S1: Schematic of all ground-state Na-vacancy configurations of binary NASICON systems considered. All schematics correspond to the primitive cell (2 formula units) of the NASICON structure. The oxygen atoms are not shown for visual clarity.

Downloaded from http://pubs.acs.org/aamick/article-supplement/5249728/pdf/am-2026-11510n_si_001/ by INDIAN INST OF SCIENCE user on 07 August 2026

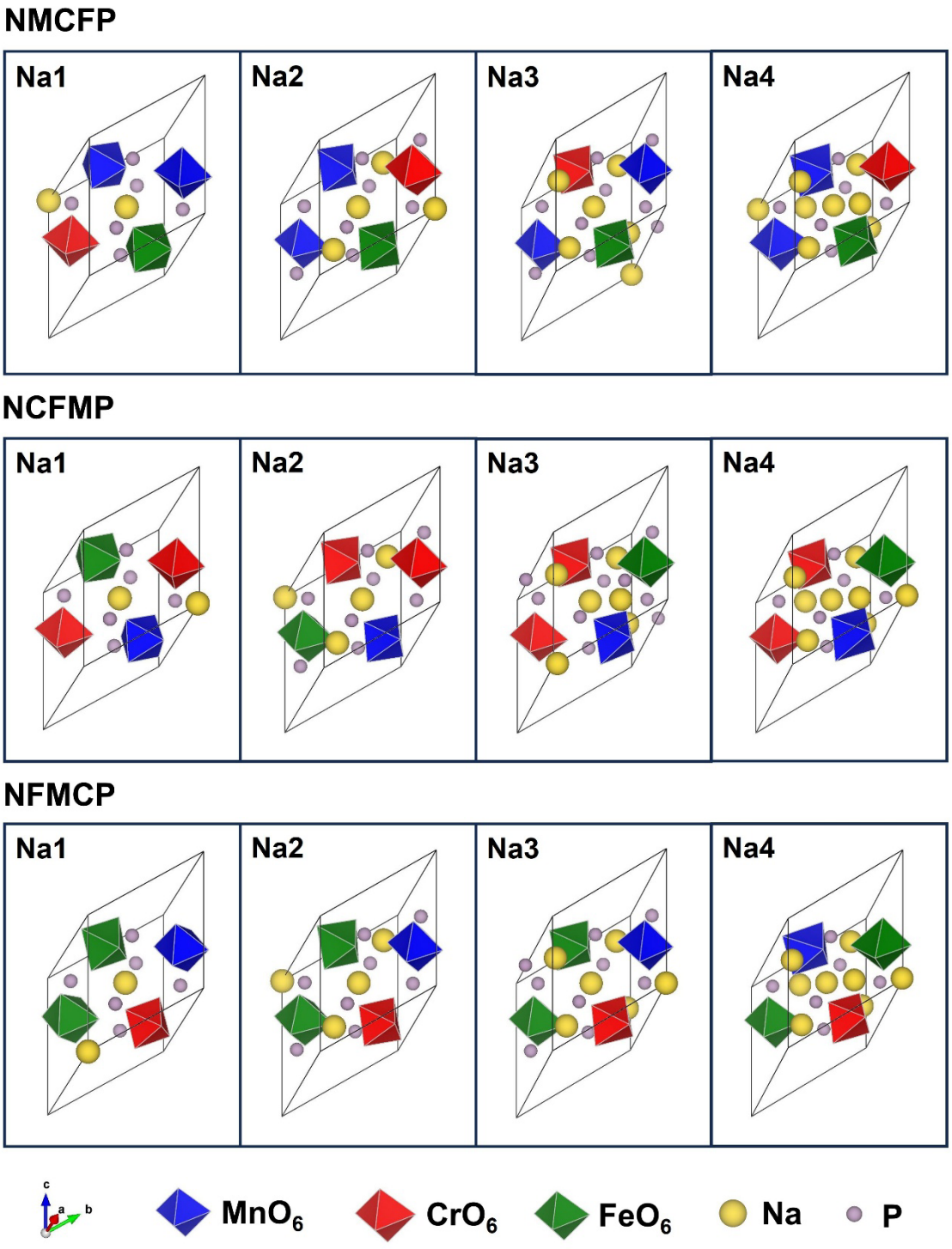

Figure S2: Schematic of all ground-state Na-vacancy configurations of ternary NASICON systems considered. Notations used are identical to **Figure S1**.

Downloaded from http://pubs.acs.org/aamick/article-supplement/5249728/pdf/am-2026-11510n_si_001/ by INDIAN INST OF SCIENCE user on 07 August 2026

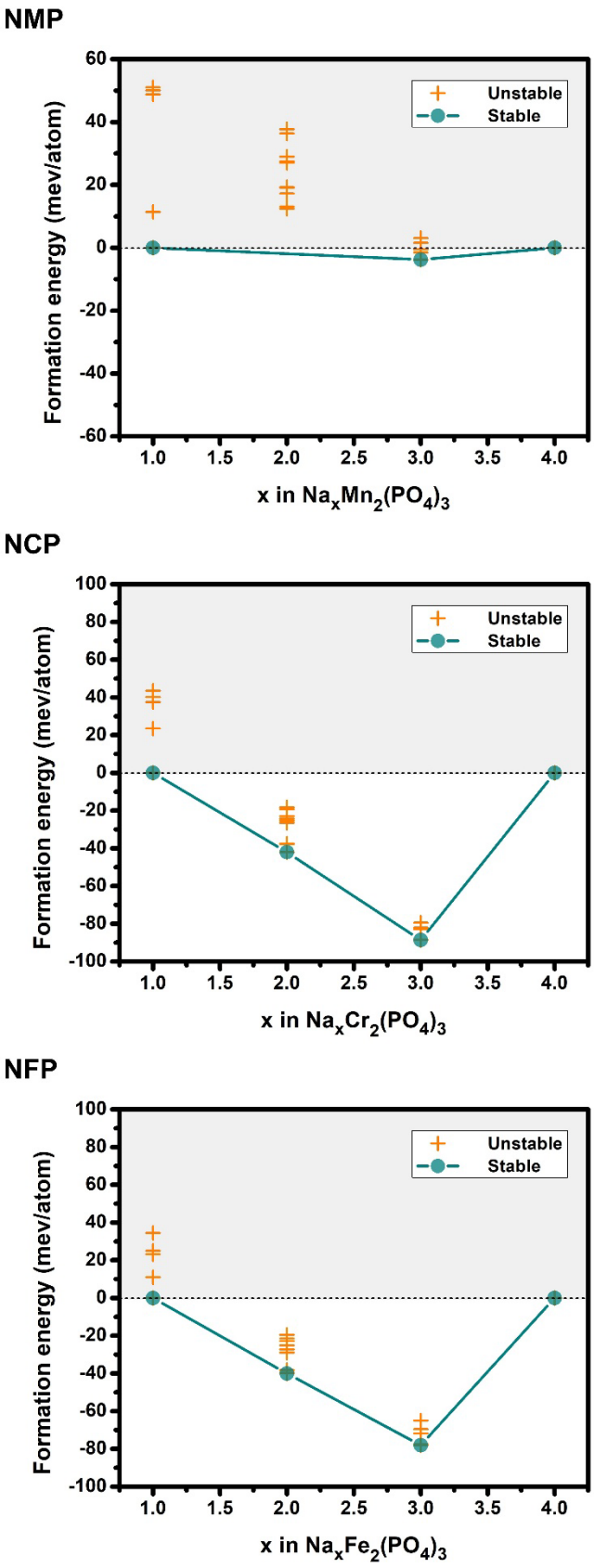

Figure S3: DFT calculated 0 K convex hull of unary NASICON cathodes considered in this work.

Downloaded from http://pubs.acs.org/aamick/article-supplement/5249728/pdf/am-2026-11510n_si_001/ by INDIAN INST OF SCIENCE user on 07 August 2026

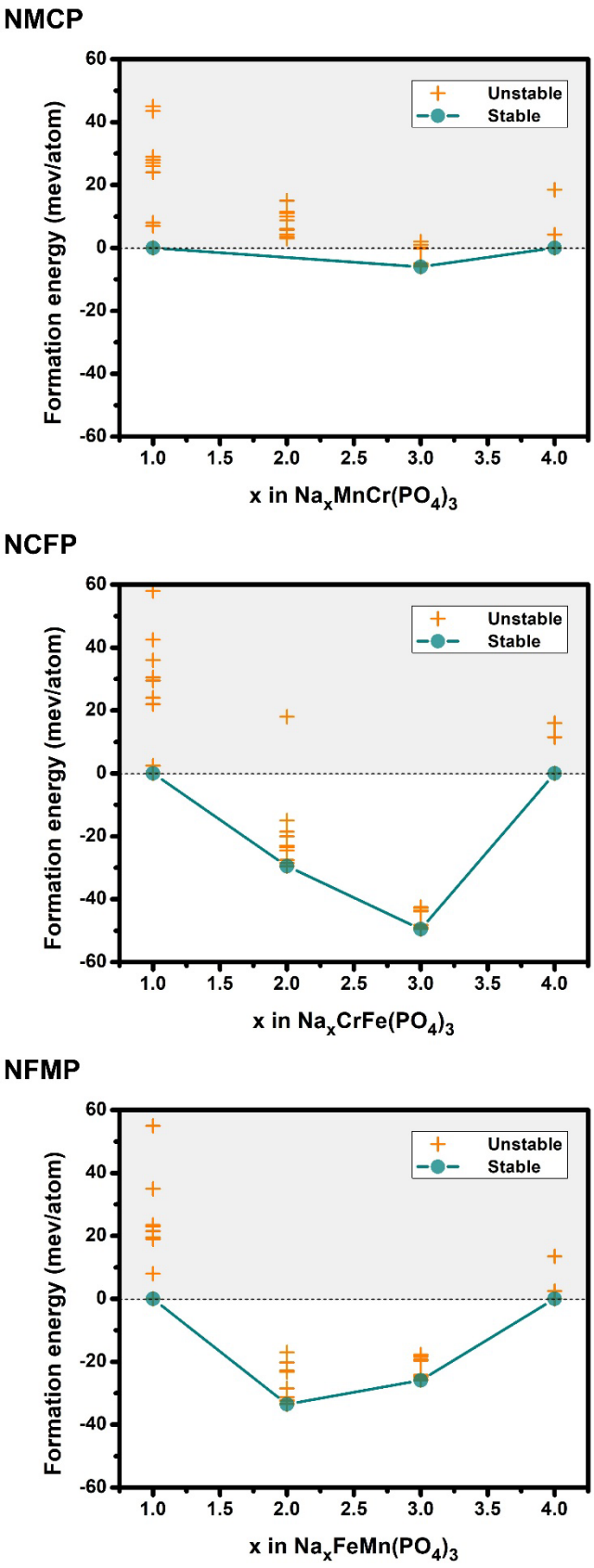

Figure S4: DFT calculated 0 K convex hull of binary NASICON cathodes considered in this work.

Downloaded from http://pubs.acs.org/aamick/article-supplement/5249728/pdf/am-2026-11510n_si_001/ by INDIAN INST OF SCIENCE user on 07 August 2026

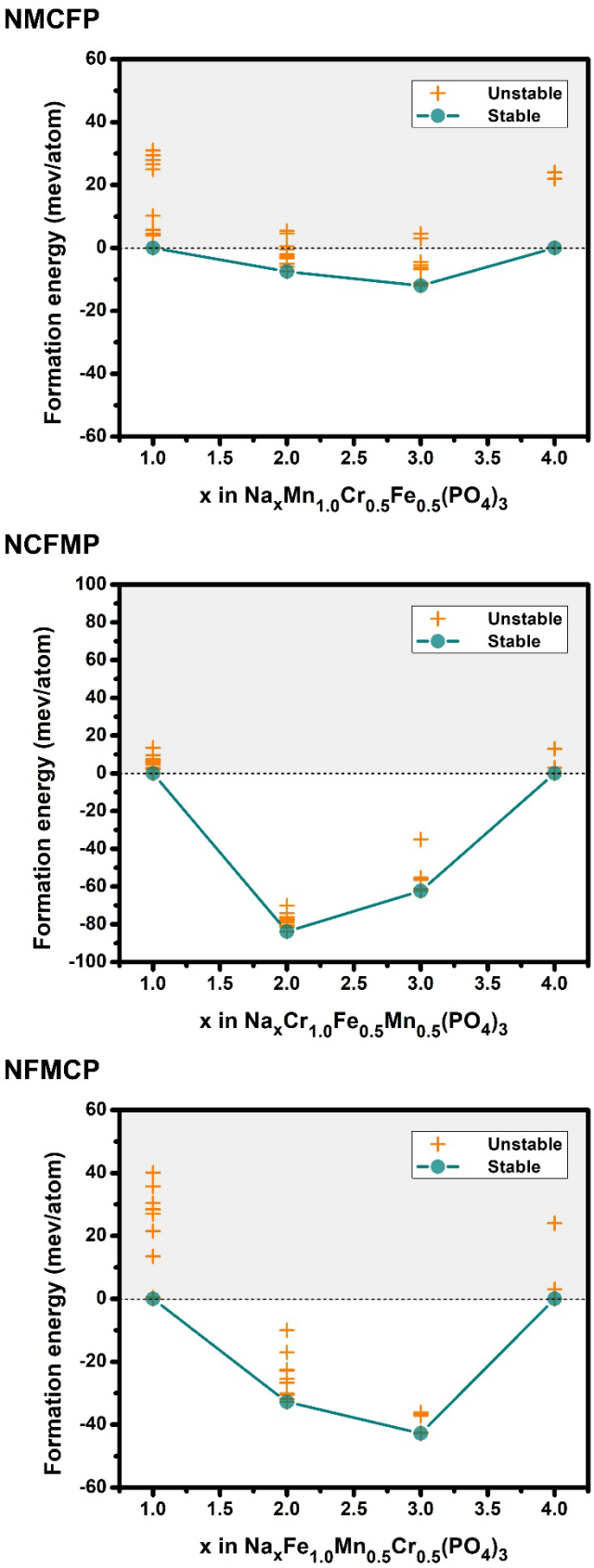

Figure S5: DFT calculated 0 K convex hull of ternary NASICON cathodes considered in this work.

Downloaded from http://pubs.acs.org/aamick/article-supplement/5249728/pdf/am-2026-11510n_si_001/ by INDIAN INST OF SCIENCE user on 07 August 2026

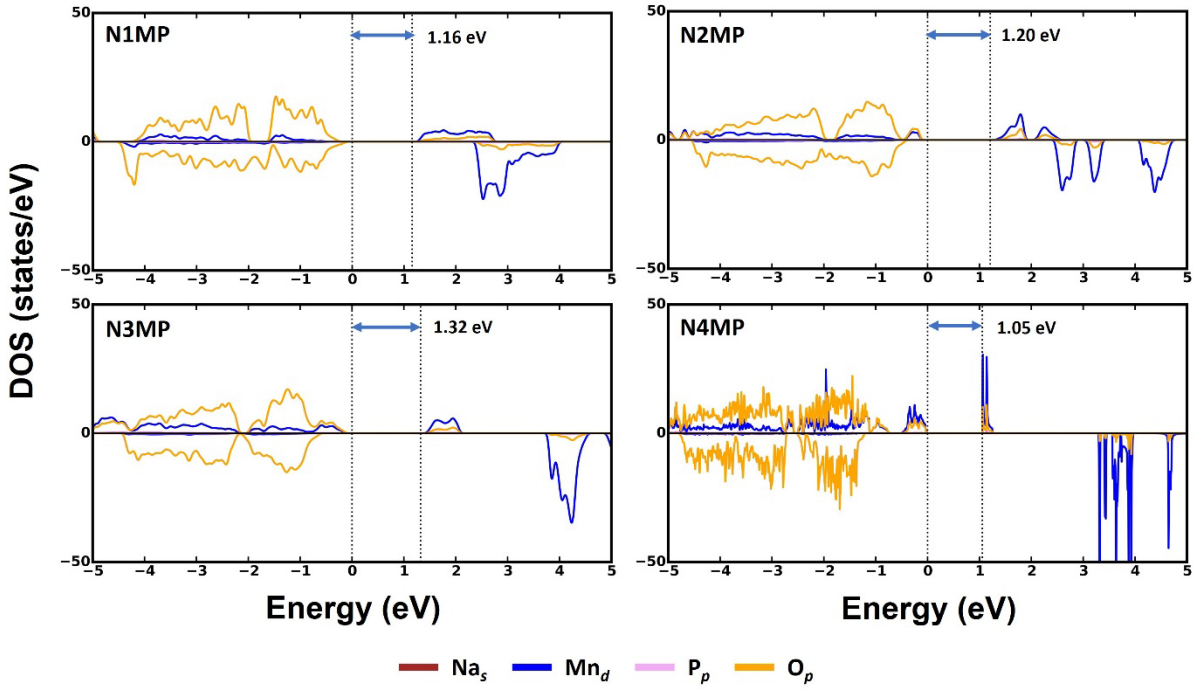

Figure S6: Atom-projected electronic DOS for different Na contents in the NMP cathode. Brown, blue, pink, and orange lines refer to Na *s*, Mn *d*, P *p*, and O *p* states, respectively. Black dotted vertical lines indicate valence and conduction band edges, with the corresponding band gap given as text notations. In case of metallic systems, the dotted vertical line refers to the Fermi energy. N1MP, N2MP, N3MP, and N4MP correspond to $NaMn_2(PO_4)_3$, $Na_2Mn_2(PO_4)_3$, $Na_3Mn_2(PO_4)_3$, and $Na_4Mn_2(PO_4)_3$ compositions.

Downloaded from http://pubs.acs.org/aamick/article-supplement/5249728/pdf/am-2026-11510n_si_001/ by INDIAN INST OF SCIENCE user on 07 August 2026

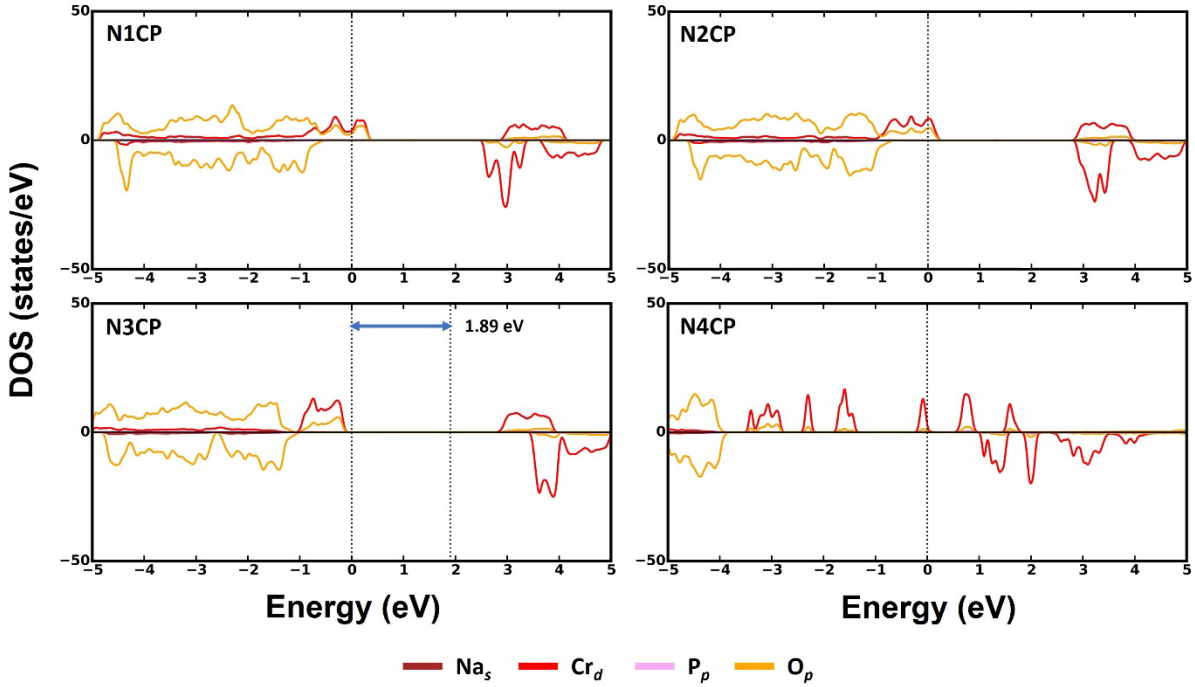

Figure S7: Atom-projected electronic DOS for different Na contents in the NCP cathode. Red lines correspond to Cr *d* states, with the remaining notations used identical to **Figure S4**. N1CP, N2CP, N3CP, and N4CP correspond to $NaCr_2(PO_4)_3$, $Na_2Cr_2(PO_4)_3$, $Na_3Cr_2(PO_4)_3$, and $Na_4Cr_2(PO_4)_3$ compositions.

Downloaded from http://pubs.acs.org/aamick/article-supplement/5249728/pdf/am-2026-11510n_si_001/ by INDIAN INST OF SCIENCE user on 07 August 2026

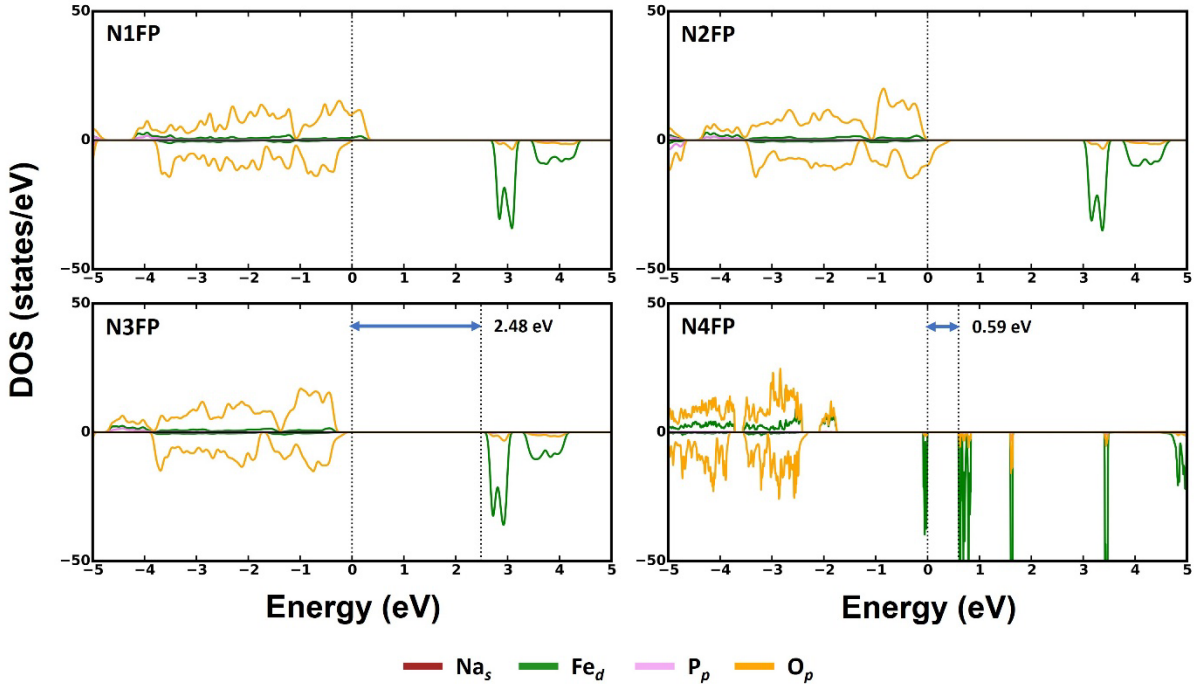

Figure S8: Atom-projected electronic DOS for different Na contents in the NFP cathode. Green lines correspond to Fe *d* states, with the remaining notations used identical to **Figure S4**. N1FP, N2FP, N3FP, and N4FP correspond to $NaFe_2(PO_4)_3$, $Na_2Fe_2(PO_4)_3$, $Na_3Fe_2(PO_4)_3$, and $Na_4Fe_2(PO_4)_3$ compositions.

Downloaded from http://pubs.acs.org/aamick/article-supplement/5249728/pdf/am-2026-11510n_si_001/ by INDIAN INST OF SCIENCE user on 07 August 2026

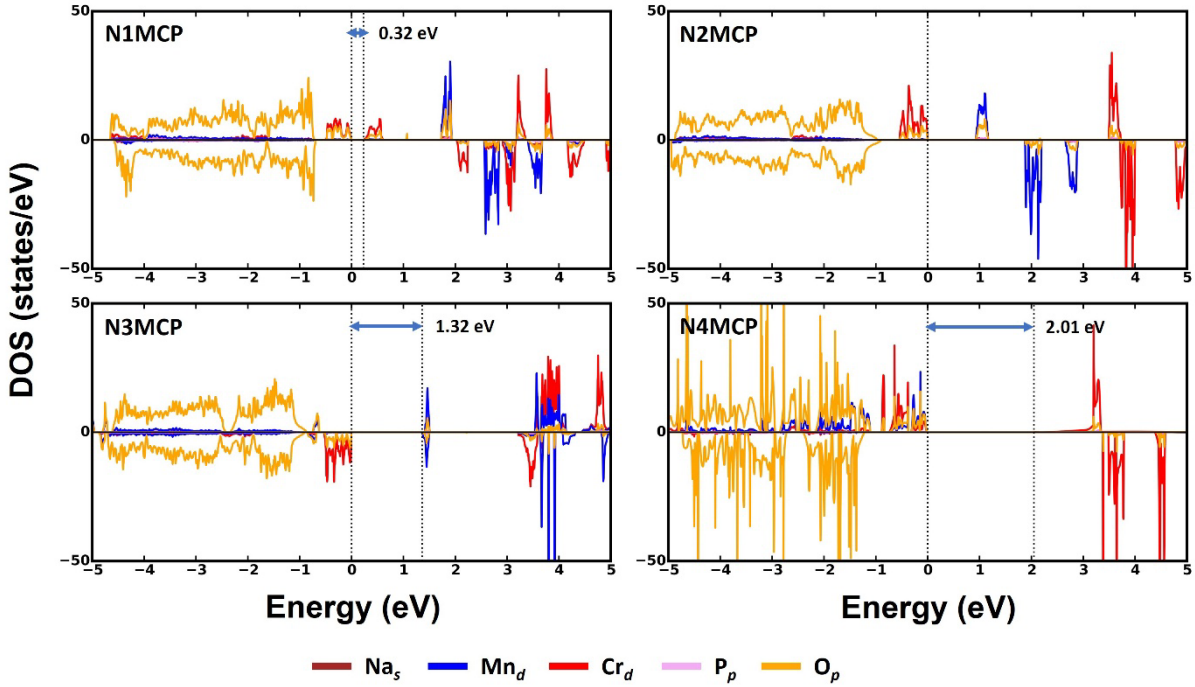

Figure S9: Atom-projected electronic DOS for different Na contents in the NMCP cathode. Notations used are identical to **Figure S4-S6**. N1MCP, N2MCP, N3MCP, and N4MCP correspond to $NaMnCr(PO_4)_3$, $Na_2MnCr(PO_4)_3$, $Na_3MnCr(PO_4)_3$, and $Na_4MnCr(PO_4)_3$ compositions.

Downloaded from http://pubs.acs.org/aamick/article-supplement/5249728/pdf/am-2026-11510n_si_001/ by INDIAN INST OF SCIENCE user on 07 August 2026

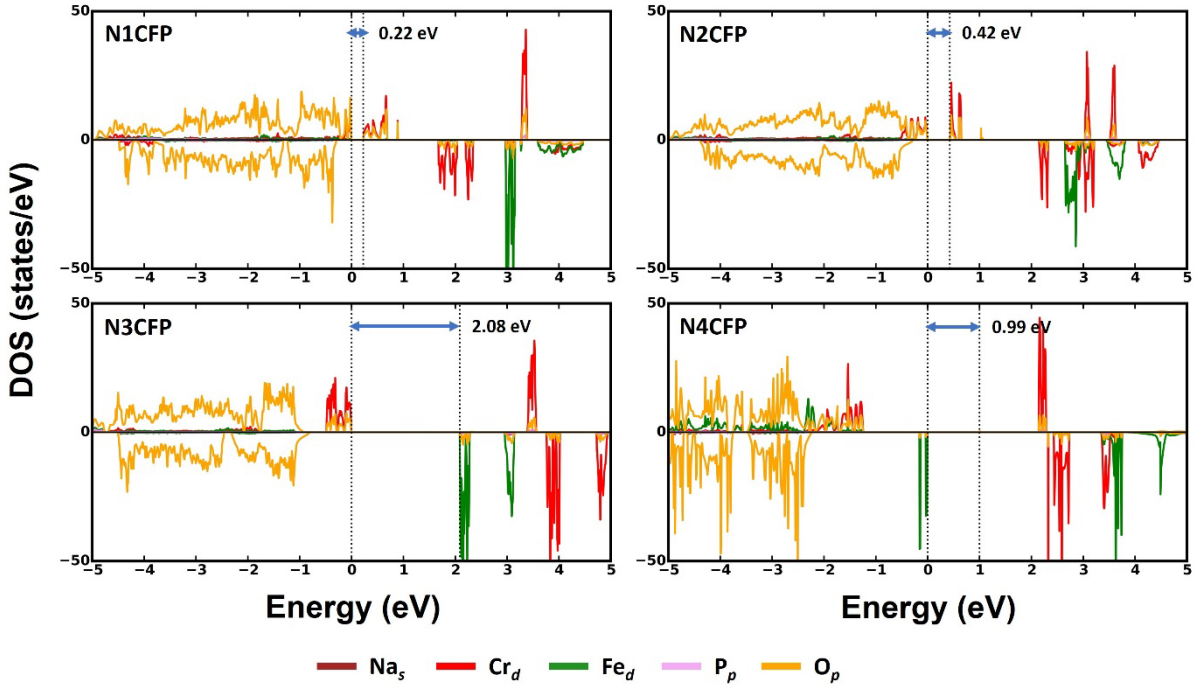

Figure S10: Atom-projected electronic DOS for different Na contents in the NCFP cathode. Notations used are identical to **Figure S4-S6**. N1CFP, N2CFP, N3CFP, and N4CFP correspond to $NaCrFe(PO_4)_3$, $Na_2CrFe(PO_4)_3$, $Na_3CrFe(PO_4)_3$, and $Na_4CrFe(PO_4)_3$ compositions.

Downloaded from http://pubs.acs.org/aamick/article-supplement/5249728/pdf/am-2026-11510n_si_001/ by INDIAN INST OF SCIENCE user on 07 August 2026

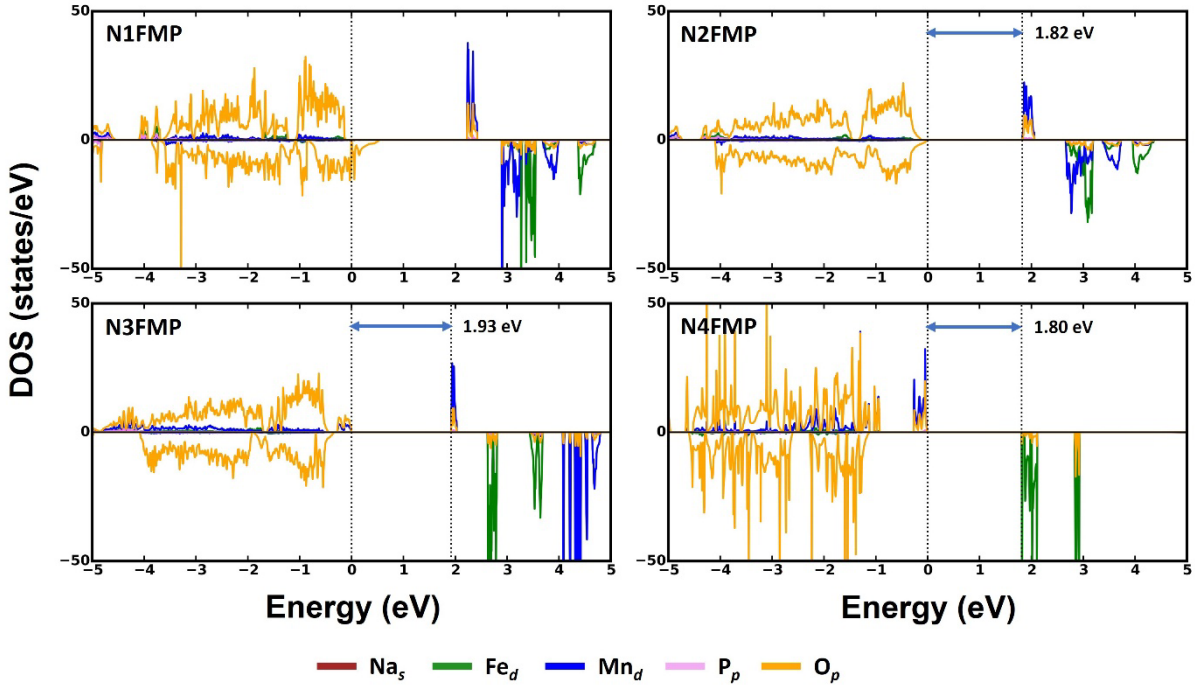

Figure S11: Atom-projected electronic DOS for different Na contents in the NFMP cathode. Notations used are identical to **Figure S4-S6**. N1FMP, N2FMP, N3FMP, and N4FMP correspond to $NaFeMn(PO_4)_3$, $Na_2FeMn(PO_4)_3$, $Na_3FeMn(PO_4)_3$, and $Na_4FeMn(PO_4)_3$ compositions.

Downloaded from http://pubs.acs.org/aamick/article-supplement/5249728/pdf/am-2026-11510n_si_001/ by INDIAN INST OF SCIENCE user on 07 August 2026

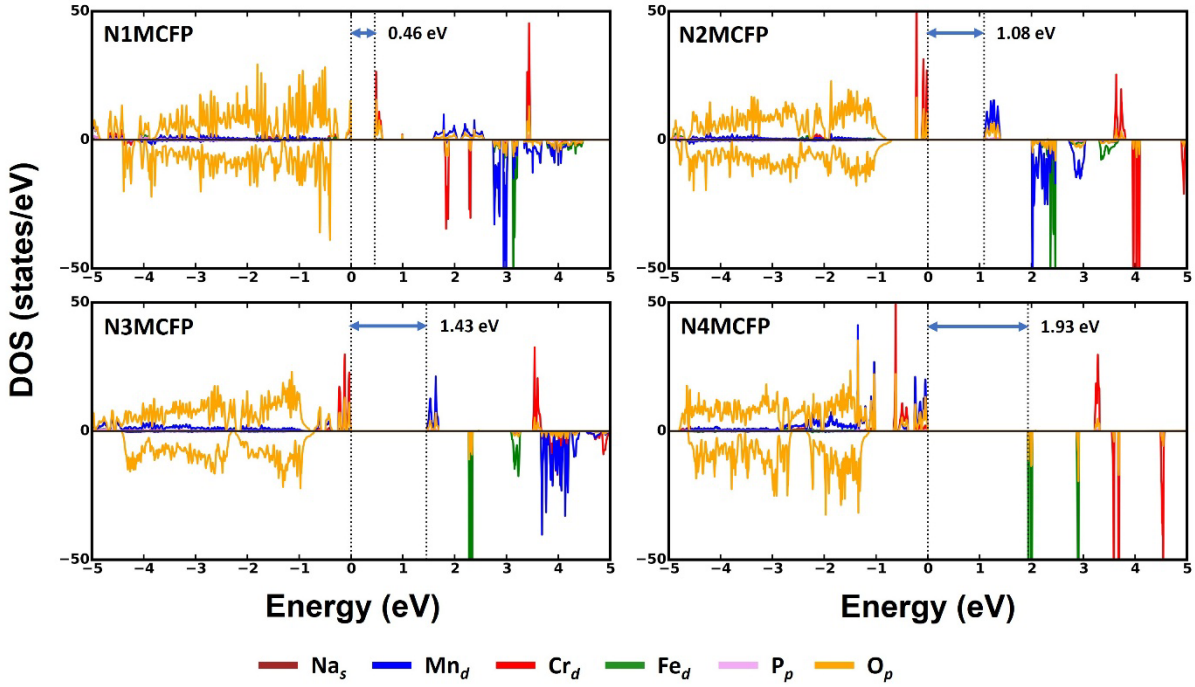

Figure S12: Atom-projected electronic DOS for different Na contents in the NMCFP cathode. Notations used are identical to **Figure S4-S6**. N1MCFP, N2MCFP, N3MCFP, and N4MCFP correspond to $NaMnCr_{0.5}Fe_{0.5}(PO_4)_3$, $Na_2MnCr_{0.5}Fe_{0.5}(PO_4)_3$, $Na_3MnCr_{0.5}Fe_{0.5}(PO_4)_3$, and $Na_4MnCr_{0.5}Fe_{0.5}(PO_4)_3$ compositions.

Downloaded from http://pubs.acs.org/aamick/article-supplement/5249728/pdf/am-2026-11510n_si_001/ by INDIAN INST OF SCIENCE user on 07 August 2026

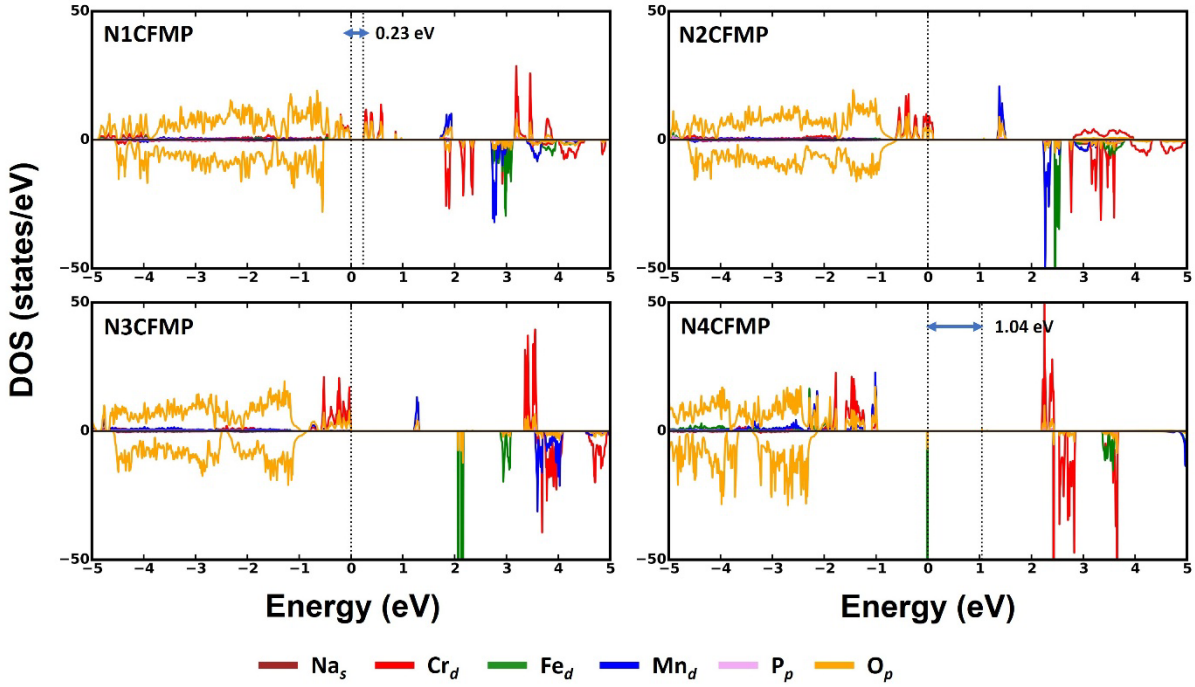

Figure S13: Atom-projected electronic DOS for different Na contents in the NCFMP cathode. Notations used are identical to **Figure S4-S6**. N1CFMP, N2CFMP, N3CFMP, and N4CFMP correspond to $NaCrFe_{0.5}Mn_{0.5}(PO_4)_3$, $Na_2CrFe_{0.5}Mn_{0.5}(PO_4)_3$, $Na_3CrFe_{0.5}Mn_{0.5}(PO_4)_3$, and $Na_4CrFe_{0.5}Mn_{0.5}(PO_4)_3$ compositions.

Downloaded from http://pubs.acs.org/aamick/article-supplement/5249728/pdf/am-2026-11510n_si_001/ by INDIAN INST OF SCIENCE user on 07 August 2026

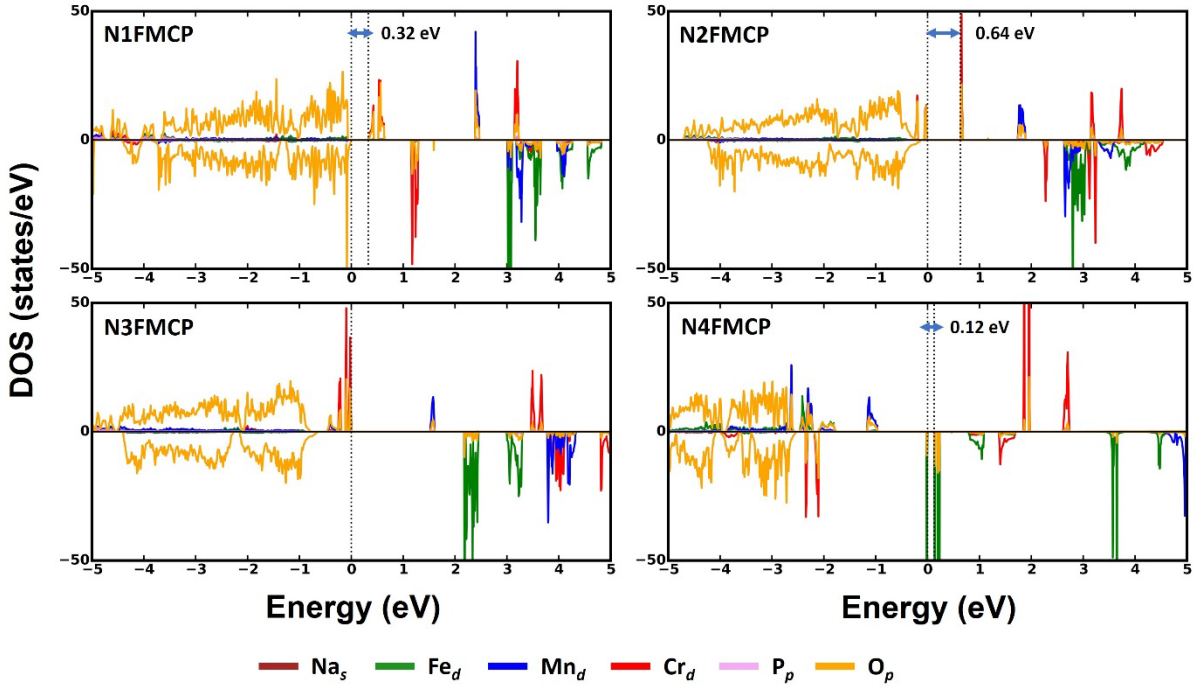

Figure S14: Atom-projected electronic DOS for different Na contents in the NFMCP cathode. Notations used are identical to **Figure S4-S6**. N1FMCP, N2FMCP, N3FMCP, and N4FMCP correspond to $NaFeMn_{0.5}Cr_{0.5}(PO_4)_3$, $Na_2FeMn_{0.5}Cr_{0.5}(PO_4)_3$, $Na_3FeMn_{0.5}Cr_{0.5}(PO_4)_3$, and $Na_4FeMn_{0.5}Cr_{0.5}(PO_4)_3$ compositions.

Downloaded from http://pubs.acs.org/aamick/article-supplement/5249728/pdf/am-2026-11510n_si_001/ by INDIAN INST OF SCIENCE user on 07 August 2026

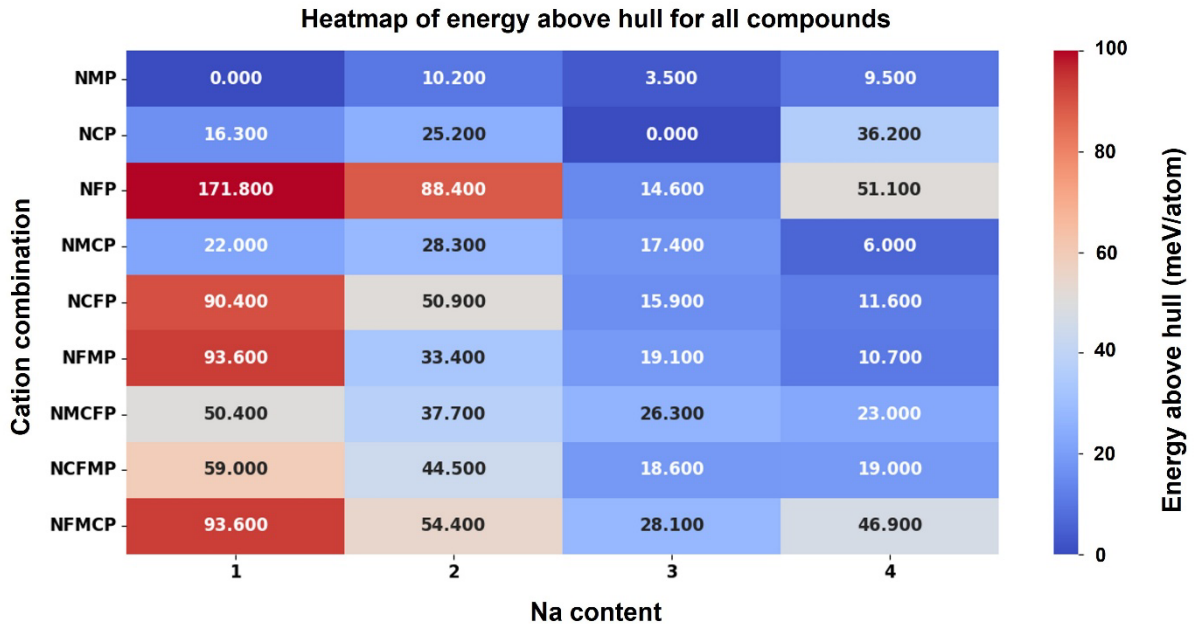

Figure S15: Heat map of E_{hull} (in meV/atom) for all unary, binary, and ternary NASICON compositions across sodium contents $1 \leq x \leq 4$. Stable phases ($E_{hull} = 0$) are shown in dark blue, metastable compositions ($E_{hull} \leq 50$ meV/atom) appear in lighter shades of blue to red, and unstable phases ($E_{hull} > 50$ meV atom^{-1}) are in saturated red. Numerical values in each cell denote the computed E_{hull} for the most stable Na/vacancy ordering at the given composition.

Downloaded from http://pubs.acs.org/aamick/article-supplement/5249728/pdf/am-2026-11510n_si_001/ by INDIAN INST OF SCIENCE user on 07 August 2026

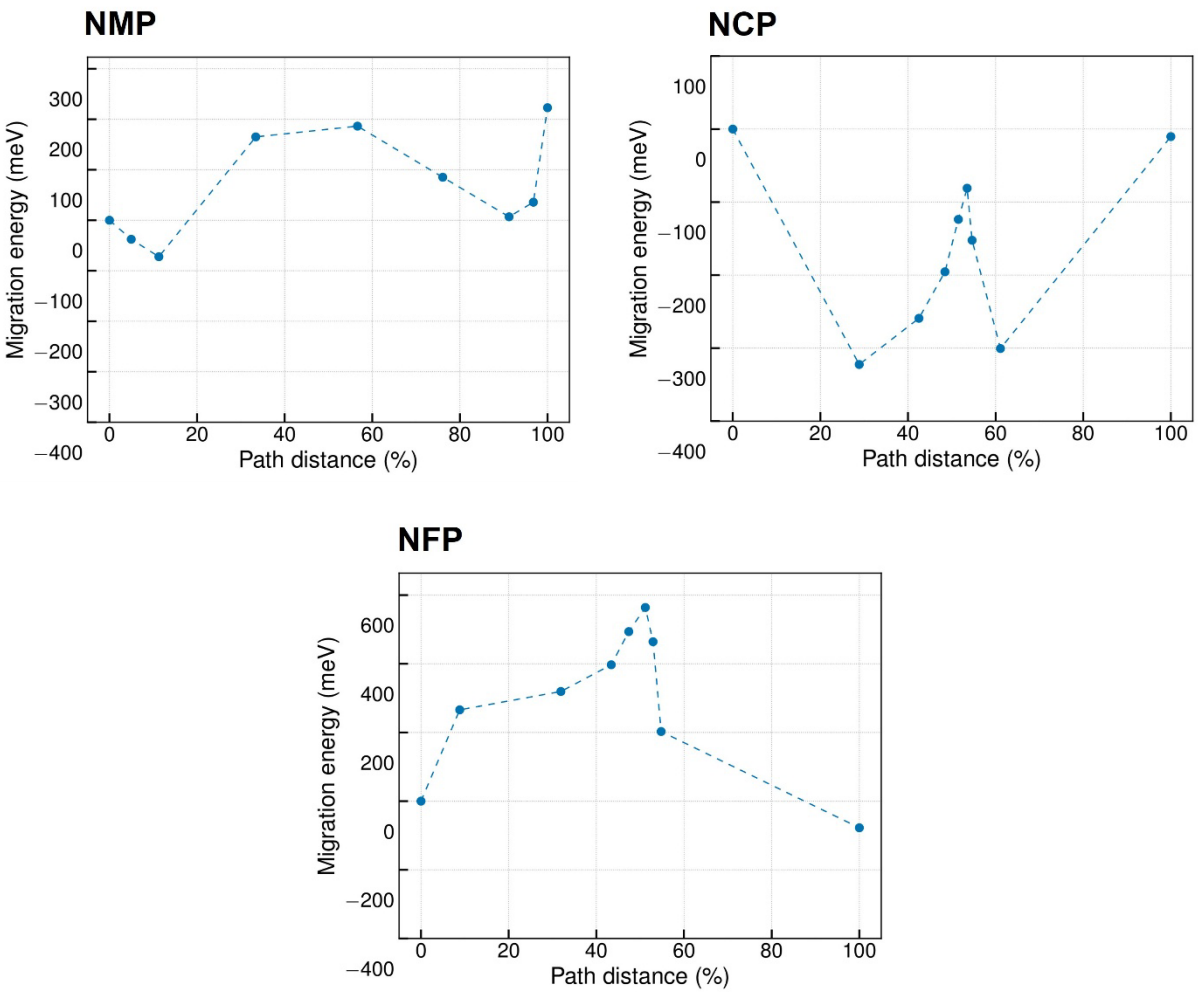

Figure S16: The minimum energy pathways (MEP), as calculated by DFT-based NEB for unary NASICON systems considered.

Downloaded from http://pubs.acs.org/aamick/article-supplement/5249728/pdf/am-2026-11510n_si_001/ by INDIAN INST OF SCIENCE user on 07 August 2026

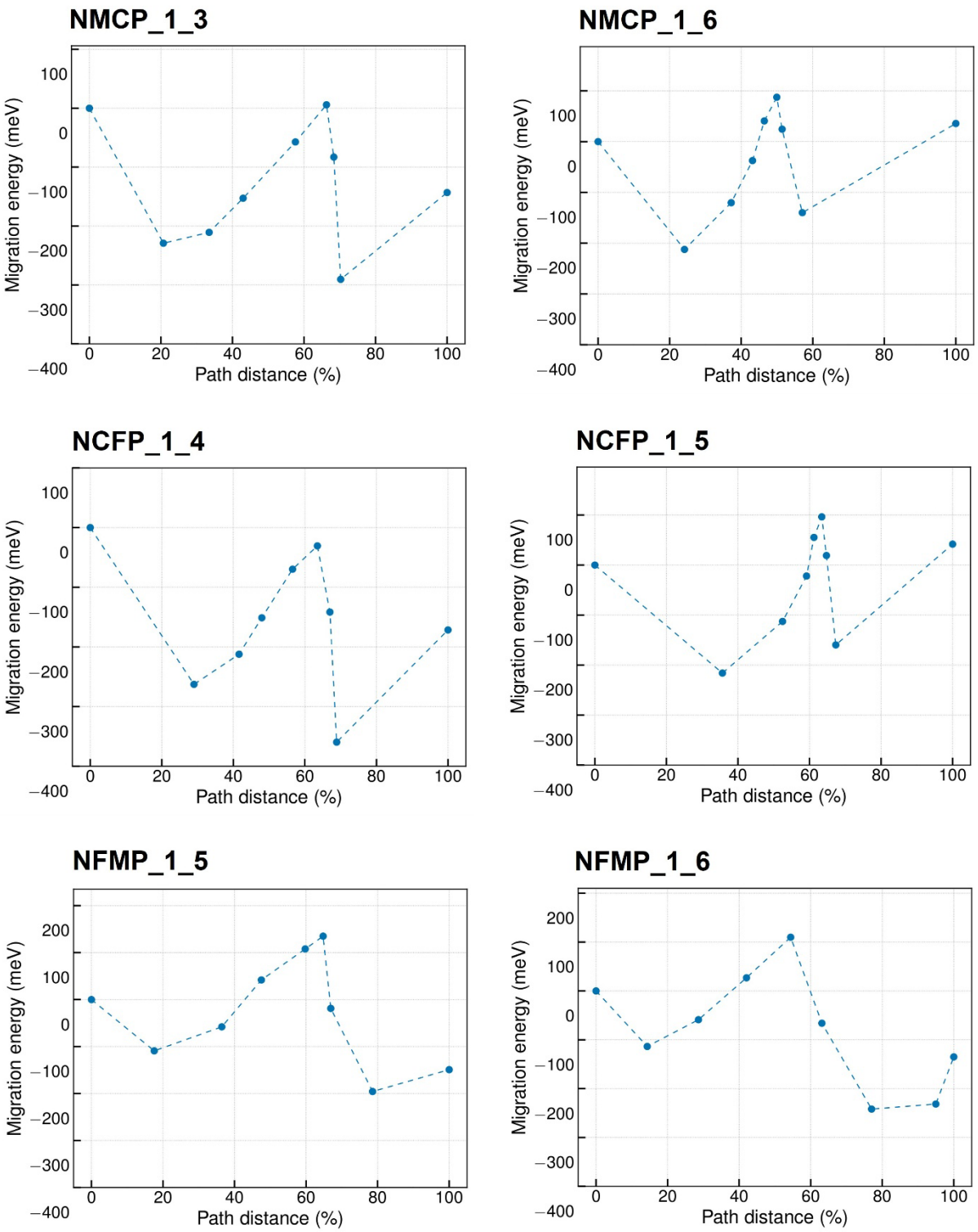

Figure S17: DFT-NEB calculated MEPs of binary NASICON cathodes for symmetrically distinct Na1–Na2 hops identified in each structure. The numerical annotations across each composition indicate the Na site indices across which a hop was simulated.

Downloaded from http://pubs.acs.org/aamick/article-supplement/5249728/pdf/am-2026-11510n_si_001/ by INDIAN INST OF SCIENCE user on 07 August 2026

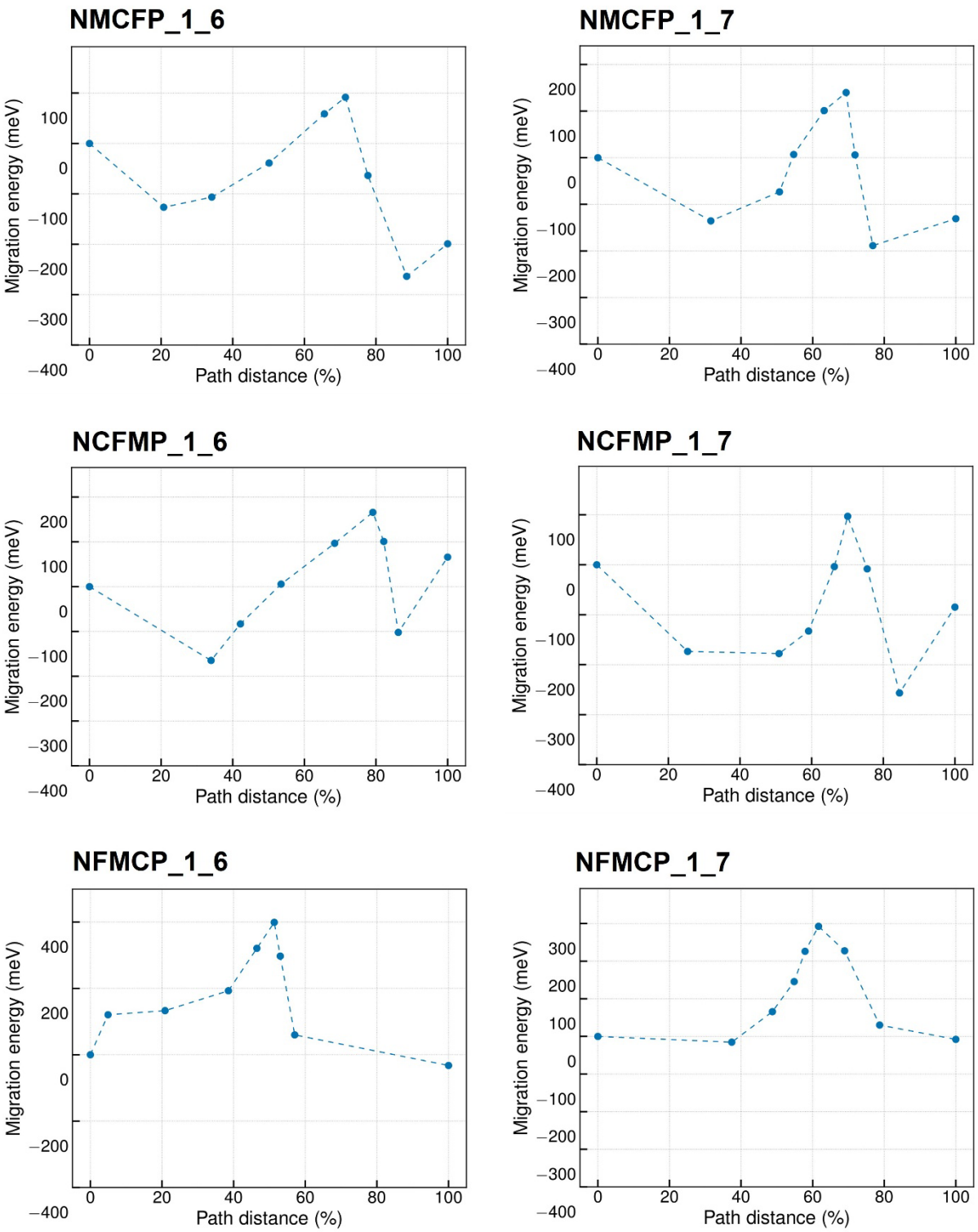

Figure S18: DFT-NEB calculated MEPs of ternary NASICON cathodes for symmetrically distinct Na1–Na2 hops identified in each structure. The numerical annotations across each composition indicate the Na site index across which a hop was simulated.

Downloaded from http://pubs.acs.org/aamick/article-supplement/5249728/pdf/am-2026-11510n_si_001/ by INDIAN INST OF SCIENCE user on 07 August 2026

References

(1) Kresse, G.; Furthmüller, J. Efficient Iterative Schemes for *Ab Initio* Total-Energy Calculations Using a Plane-Wave Basis Set. *Phys. Rev. B* **1996**, *54* (16), 11169–11186. https://doi.org/10.1103/PhysRevB.54.11169.

(2) Kresse, G.; Furthmüller, J. Efficiency of Ab-Initio Total Energy Calculations for Metals and Semiconductors Using a Plane-Wave Basis Set. *Computational Materials Science* **1996**, *6* (1), 15–50. https://doi.org/10.1016/0927-0256(96)00008-0.

(3) Kresse, G.; Joubert, D. From Ultrasoft Pseudopotentials to the Projector Augmented-Wave Method. *Phys. Rev. B* **1999**, *59* (3), 1758–1775. https://doi.org/10.1103/PhysRevB.59.1758.

(4) Blöchl, P. E. Projector Augmented-Wave Method. *Phys. Rev. B* **1994**, *50* (24), 17953–17979. https://doi.org/10.1103/PhysRevB.50.17953.

(5) Sun, J.; Ruzsinszky, A.; Perdew, J. P. Strongly Constrained and Appropriately Normed Semilocal Density Functional. *Phys. Rev. Lett.* **2015**, *115* (3), 036402. https://doi.org/10.1103/PhysRevLett.115.036402.

(6) Anisimov, V. I.; Zaanen, J.; Andersen, O. K. Band Theory and Mott Insulators: Hubbard *U* Instead of Stoner *I*. *Phys. Rev. B* **1991**, *44* (3), 943–954. https://doi.org/10.1103/PhysRevB.44.943.

(7) Sai Gautam, G.; Carter, E. A. Evaluating Transition Metal Oxides within DFT-SCAN and SCAN + U Frameworks for Solar Thermochemical Applications. *Phys. Rev. Materials* **2018**, *2* (9), 095401. https://doi.org/10.1103/PhysRevMaterials.2.095401.

(8) Long, O. Y.; Sai Gautam, G.; Carter, E. A. Evaluating Optimal U for 3 d Transition-Metal Oxides within the SCAN+ U Framework. *Phys. Rev. Materials* **2020**, *4* (4), 045401. https://doi.org/10.1103/PhysRevMaterials.4.045401.

(9) Swathilakshmi, S.; Devi, R.; Sai Gautam, G. Performance of the r ^{2} SCAN Functional in Transition Metal Oxides. *J. Chem. Theory Comput.* **2023**, *19* (13), 4202–4215. https://doi.org/10.1021/acs.jctc.3c00030.

(10) Hellenbrandt, M. The Inorganic Crystal Structure Database (ICSD)—Present and Future. *Crystallography Reviews* **2004**, *10* (1), 17–22. https://doi.org/10.1080/08893110410001664882.

(11) Monkhorst, H. J.; Pack, J. D. Special Points for Brillouin-Zone Integrations. *Phys. Rev. B* **1976**, *13* (12), 5188–5192. https://doi.org/10.1103/PhysRevB.13.5188.

(12) Blöchl, P. E.; Jepsen, O.; Andersen, O. K. Improved Tetrahedron Method for Brillouin-Zone Integrations. *Phys. Rev. B* **1994**, *49* (23), 16223–16233. https://doi.org/10.1103/PhysRevB.49.16223.

(13) Aydinol, M. K.; Kohan, A. F.; Ceder, G.; Cho, K.; Joannopoulos, J. *Ab Initio* Study of Lithium Intercalation in Metal Oxides and Metal Dichalcogenides. *Phys. Rev. B* **1997**, *56* (3), 1354–1365. https://doi.org/10.1103/PhysRevB.56.1354.

(14) Ong, S. P.; Richards, W. D.; Jain, A.; Hautier, G.; Kocher, M.; Cholia, S.; Gunter, D.; Chevrier, V. L.; Persson, K. A.; Ceder, G. Python Materials Genomics (Pymatgen): A Robust, Open-Source Python Library for Materials Analysis. *Computational Materials Science* **2013**, *68*, 314–319. https://doi.org/10.1016/j.commatsci.2012.10.028.

(15) Ewald, P. P. Die Berechnung Optischer Und Elektrostatischer Gitterpotentiale. *Annalen der Physik* **1921**, *369* (3), 253–287. https://doi.org/10.1002/andp.19213690304.

(16) Batatia, I.; Benner, P.; Chiang, Y.; Elena, A. M.; Kovács, D. P.; Riebesell, J.; Advincula, X. R.; Asta, M.; Avaylon, M.; Baldwin, W. J.; Berger, F.; Bernstein, N.; Bhowmik, A.; Blau, S. M.; Cărare, V.; Darby, J. P.; De, S.; Della Pia, F.; Deringer, V. L.; Elijošius, R.; El-Machachi, Z.; Falcioni, F.; Fako, E.; Ferrari, A. C.; Genreith-Schriever, A.; George, J.; Goodall, R. E. A.; Grey, C. P.; Grigorev, P.; Han, S.; Handley, W.; Heenen, H. H.; Hermansson, K.; Holm, C.; Jaafar, J.; Hofmann, S.; Jakob, K. S.; Jung, H.; Kapil, V.; Kaplan, A. D.; Karimitari, N.; Kermode, J. R.; Kroupa, N.; Kullgren, J.; Kuner, M. C.; Kuryla, D.; Liepuoniute, G.; Margraf, J. T.; Magdău, I.-B.; Michaelides, A.; Moore, J. H.; Naik, A. A.; Niblett, S. P.; Norwood, S. W.; O'Neill, N.; Ortner, C.; Persson, K. A.; Reuter, K.; Rosen, A. S.; Schaaf, L. L.; Schran, C.; Shi, B. X.; Sivonxay, E.; Stenczel, T. K.; Svahn, V.; Sutton, C.; Swinburne, T. D.; Tilly, J.; van der Oord, C.; Varga-Umbrich, E.; Vegge, T.; Vondrák, M.; Wang, Y.; Witt, W. C.; Zills, F.; Csányi, G. A Foundation Model for Atomistic Materials Chemistry. arXiv 2024. https://doi.org/10.48550/ARXIV.2401.00096.

(17) Hjorth Larsen, A.; Jørgen Mortensen, J.; Blomqvist, J.; Castelli, I. E.; Christensen, R.; Dułak, M.; Friis, J.; Groves, M. N.; Hammer, B.; Hargus, C.; Hermes, E. D.; Jennings, P. C.; Bjerre Jensen, P.; Kermode, J.; Kitchin, J. R.; Leonhard Kolsbjerg, E.; Kubal, J.; Kaasbjerg, K.; Lysgaard, S.; Bergmann Maronsson, J.; Maxson, T.; Olsen, T.; Pastewka, L.; Peterson, A.; Rostgaard, C.; Schiøtz, J.; Schütt, O.; Strange, M.; Thygesen, K. S.; Vegge, T.; Vilhelmsen, L.; Walter, M.; Zeng, Z.; Jacobsen, K. W. The Atomic Simulation Environment—a Python Library for Working with Atoms. *J. Phys.: Condens. Matter* **2017**, *29* (27), 273002. https://doi.org/10.1088/1361-648X/aa680e.

(18) Jónsson, H.; Mills, G.; Jacobsen, K. W. Nudged Elastic Band Method for Finding Minimum Energy Paths of Transitions. In *Classical and Quantum Dynamics in Condensed Phase Simulations*; WORLD SCIENTIFIC: LERICI, Villa Marigola, 1998; pp 385–404. https://doi.org/10.1142/9789812839664_0016.

Downloaded from http://pubs.acs.org/aamick/article-supplement/5249728/pdf/am-2026-11510n_si_001/ by INDIAN INST OF SCIENCE user on 07 August 2026

(19) Smidstrup, S.; Pedersen, A.; Stokbro, K.; Jónsson, H. Improved Initial Guess for Minimum Energy Path Calculations. *The Journal of Chemical Physics* **2014**, *140* (21), 214106. https://doi.org/10.1063/1.4878664.
(20) Bheemaguli, A. K.; Xiao, P.; Sai Gautam, G. Evaluation of Foundational Machine Learned Interatomic Potentials for Migration Barrier Predictions. *Digital Discovery* **2025**, 10.1039.D5DD00534E. https://doi.org/10.1039/D5DD00534E.
(21) Henkelman, G.; Uberuaga, B. P.; Jónsson, H. A Climbing Image Nudged Elastic Band Method for Finding Saddle Points and Minimum Energy Paths. *The Journal of Chemical Physics* **2000**, *113* (22), 9901–9904. https://doi.org/10.1063/1.1329672.
(22) Shanno, D. F. Conditioning of Quasi-Newton Methods for Function Minimization. *Mathematics of computation* **1970**, *24* (111), 647–656.
(23) Perdew, J. P.; Burke, K.; Ernzerhof, M. Generalized Gradient Approximation Made Simple. *Phys. Rev. Lett.* **1996**, *77* (18), 3865–3868. https://doi.org/10.1103/PhysRevLett.77.3865.
(24) Devi, R.; Singh, B.; Canepa, P.; Sai Gautam, G. Effect of Exchange-Correlation Functionals on the Estimation of Migration Barriers in Battery Materials. *npj Comput Mater* **2022**, *8* (1), 160. https://doi.org/10.1038/s41524-022-00837-0.
(25) Singh, B.; Wang, Z.; Park, S.; Gautam, G. S.; Chotard, J.-N.; Croguennec, L.; Carlier, D.; Cheetham, A. K.; Masquelier, C.; Canepa, P. A Chemical Map of NaSICON Electrode Materials for Sodium-Ion Batteries. *J. Mater. Chem. A* **2021**, *9* (1), 281–292. https://doi.org/10.1039/D0TA10688G.
(26) Kawai, K.; Zhao, W.; Nishimura, S.; Yamada, A. High-Voltage Cr^{4+} /Cr^{3+} Redox Couple in Polyanion Compounds. *ACS Appl. Energy Mater.* **2018**, *1* (3), 928–931. https://doi.org/10.1021/acsaem.7b00105.
(27) Rajagopalan, R.; Chen, B.; Zhang, Z.; Wu, X.; Du, Y.; Huang, Y.; Li, B.; Zong, Y.; Wang, J.; Nam, G.; Sindoro, M.; Dou, S. X.; Liu, H. K.; Zhang, H. Improved Reversibility of Fe^{3+} /Fe^{4+} Redox Couple in Sodium Super Ion Conductor Type Na_3 Fe_2 $(PO_4)_3$ for Sodium-Ion Batteries. *Advanced Materials* **2017**, *29* (12), 1605694. https://doi.org/10.1002/adma.201605694.
(28) Zhao, Y.; Gao, X.; Gao, H.; Dolocan, A.; Goodenough, J. B. Elevating Energy Density for Sodium-Ion Batteries through Multielectron Reactions. *Nano Lett.* **2021**, *21* (5), 2281–2287. https://doi.org/10.1021/acs.nanolett.1c00100.
(29) Moutchou, S. E.; Fkhar, L.; Oubaha, H.; Harfouche, M.; Boschini, F.; Mahmoud, A.; Sabi, N.; Aziam, H.; Youcef, H. B. Insights on Novel Carbon-Coated NaSICON-Type Structure Na3FeCr(PO4)3@C as Positive Electrode Material for Sodium-Ion Batteries. *Electrochimica Acta* **2026**, *570*, 148949. https://doi.org/10.1016/j.electacta.2026.148949.
(30) Wang, X.; Gu, Z.; Liu, Y.; Zhao, X.; Li, K.; Cao, J.; Dong, F.; Heng, Y.; Yang, J.; Wu, X. From Inert to Active: Breaking Mott-localization Enables High Na-Storage Performance in Na_4 $MnFe(PO_4)_3$ -based Cathode. *Advanced Materials* **2026**, *38* (26), e73020. https://doi.org/10.1002/adma.73020.
(31) Gokulnath, S.; Krishnan, S.; Yadav, V.; Sathish, M. Insights and Nanoarchitectonics in Fe-Substituted Newer NaSICON Na_4 Mn_x Fe_y Cr_z $(PO_4)_3$ Cathodes for Sodium-Ion Batteries. *Energy Fuels* **2024**, *38* (14), 13407–13415. https://doi.org/10.1021/acs.energyfuels.4c02196.

Downloaded from http://pubs.acs.org/aamick/article-supplement/5249728/pdf/am-2026-11510n_si_001/ by INDIAN INST OF SCIENCE user on 07 August 2026